International Symposium
On Turbulence and Shear Flow
Phenomena (TSFP-8)
August 28 - 30, 2013 Poitiers, France

EVOLUTION OF TURBULENT FLOW STRUCTURES GENERATED BY FRACTAL GRIDS

Rafael Gomes Fernandes
Turbulence, Mixing and Flow Control Group
Department of Aeronautics, Imperial College London
London, SW7 2AZ, United Kingdom
r.g.fernandes@imperial.ac.uk

Bharathram Ganapathisubramani
Aerodynamics & Flight Mechanics Research Group
Faculty of Engineering and the Environment, University of Southampton
Southampton, SO17 1BJ, United Kingdom
g.bharath@soton.ac.uk

J. Christos Vassilicos
Turbulence, Mixing and Flow Control Group
Department of Aeronautics, Imperial College London
London, SW7 2AZ, United Kingdom
j.c.vassilicos@imperial.ac.uk

ABSTRACT

An experimental study involving a space-filling square fractal grid is presented. Using time-resolved stereoscopic Particle Image Velocimetry and Taylor's hypothesis, all components of the velocity gradient tensor are determined in three regions along the centreline of this spatially developing flow: where turbulence is produced, at the turbulence intensity peak and in the decay region. Some of the acclaimed universal aspects of small-scale turbulence are shown to be the result of an evolution process over a considerable streamwise extent of the flow. The spatial evolution of the second (Q) and third (R) velocity gradient invariants is presented and the related characteristic "universal tear-drop" shape is only fully established at the most downstream location. A similar evolution is seen in the alignments between vorticity and the eigenvectors of the strain rate tensor where, in the production region, vortex stretching is only slightly favoured over compression.

INTRODUCTION

Results from Seoud & Vassilicos (2007), Mazellier & Vassilicos (2010), Valente & Vassilicos (2011), Valente & Vassilicos (2012), Gomes-Fernandes *et al.* (2012), Discetti *et al.* (2013) and Nagata *et al.* (2013) show that there is well defined turbulent flow region downstream of space-filling fractal square grids and regular grids where the ratio of the integral length scale L to the Taylor microscale λ remains approximately constant as the Reynolds number $Re_\lambda = u'\lambda/\nu$ decays (u' is the root mean square of the velocity fluctuations and ν is the kinematic viscosity). This fact implies (see aforementioned references) that the dimensionless dissipation constant, C_ε, defined by $\varepsilon = C_\varepsilon u'^3/L$ (where ε is the kinetic energy dissipation rate per unit mass) is not constant as it is usually assumed to be at high enough Reynolds numbers. Instead it increases as Re_λ decays like $C_\varepsilon \approx Re_\lambda^{-1}$. Even so, the flow in the region where this dissipative behaviour is observed is approximately isotropic and has a well-defined power law energy spectrum over a wide range with exponent very close to -5/3.

Before the discovery of this flow region where C_ε takes this unusual scaling, the work of Hurst & Vassilicos (2007) revealed some interesting characteristics of flow generated by space-filling fractal square grids and in particular a protracted turbulence production region in the centreline. In this region, the turbulent structures are formed and turbulence intensity is produced and increasing. The length of this region is usually small in the kinds of regular grids customarily used for increasing homogeneity, but for the space-filling fractal square grids this length is considerable.

Hence, in order to obtain more insight on these unusual results, it is useful to study the behaviour of the velocity derivatives and flow structures. This type of study allows us to get insight on how statistics of energy dissipation are formed and their dependence on vorticity and strain rate dynamics. To that end, an experiment on turbulence generated by a fractal square grid was conducted using Particle Image Velocimetry and a water channel.

EXPERIMENTAL SETUP

The same experimental facility and flow conditions as Gomes-Fernandes *et al.* (2012) were used to perform an experiment on the water flow generated by a space-filling frac-

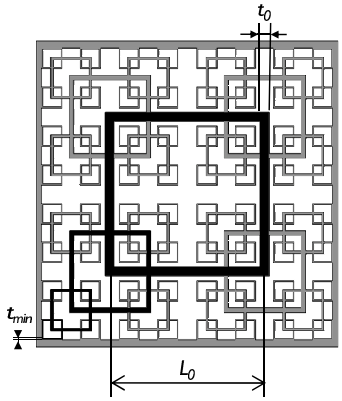

Figure 1. Space filling square fractal grid (SFG) geometry after Gomes-Fernandes *et al.* (2012). The "fractal iterations" parameter (N) is the number of times the square shape is repeated at different scales. Here $N = 4$. Note that the streamwise thickness of all the bars in the grid is the same.

tal square grid denoted SFG17 (see schematic in figure 1). This grid has four "fractal iterations" (N), it is characterized by having a thickness ratio, t_r, of 17 (where $t_r = t_0/t_{min}$, t_0 is the spanwise thickness of the thickest bar and t_{min} is the spanwise thickness of the thinnest bar) and has a blockage ratio of 25%. The free-stream velocity (U_∞) was set at 0.48 m/s (case A of Gomes-Fernandes *et al.* (2012)) and measurements were taken at 3 different locations at the centreline in the streamwise direction (x) of the water channel: at $x/x_*^{peak} = 0.57$ which is in the production region, at $x/x_*^{peak} = 0.94$ near the peak of turbulence intensity and at $x/x_*^{peak} = 2.04$ in the decay region (x_*^{peak} is an estimator of the turbulence intensity peak location according to Gomes-Fernandes *et al.* (2012) and an improvement on the wake-interaction length-scale introduced by Mazellier & Vassilicos (2010)). It is worth highlighting that in physical coordinates the measurement locations in the streamwise direction for the three aforementioned flow regions are 0.8, 1.3 and 2.8 m downstream of the fractal grid. This is important because the phenomena described in this paper and taking place in the production and peak locations are not just transitional and therefore of minor importance. In fact, they occur over a considerable length which can even be elongated or shortened depending on the size and design of the fractal grid (for this purpose see Gomes-Fernandes *et al.* (2012)).

Time-resolved Stereo Particle Image Velocimetry (SPIV) was the experimental technique used following the procedure outlined in Ganapathisubramani *et al.* (2007). The light sheet was set perpendicular to the flow direction where, in a plane, the three components of velocity were measured with a frequency of 2.2 kHz. Taylor's hypothesis was applied based on the distribution of the mean velocity in the measurement plane in order to compute the velocity gradients in streamwise direction ($\partial/\partial x = -1/U_c(y,z)\partial/\partial t$). To eliminate some of the noise present in the data, the velocity field was smoothed at each measured location with a 3D Gaussian filter with half-width equal to the resolution at that location. The final resolution in terms of the Kolmogorov microscale η is presented in table 1. It depends on the flow region and whether it is a streamwise (x direction) or a spanwise (y and z plane) component. The resolution in the y and z plane is based on the size of the PIV interrogation window.

Table 1. Experiment resolution.

Station	x direction	y and z plane
$x/x_*^{peak} = 0.57$	1.8η	4.3η
$x/x_*^{peak} = 0.94$	1.7η	4.8η
$x/x_*^{peak} = 2.04$	1.3η	3.4η

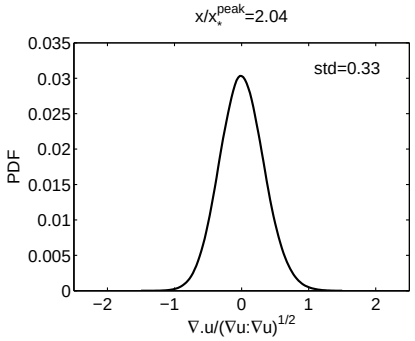

Figure 2. PDF of the divergence of the velocity field normalized by the norm of the velocity gradient tensor in the decay region.

The accuracy of the measured velocity gradients is assessed by computing the divergence of the velocity field ($\nabla.\mathbf{u}$). Figure 2 shows the PDF of $\nabla.\mathbf{u}$ normalized by the norm of the velocity gradient tensor at $x/x_*^{peak} = 2.04$. The standard deviation of this PDF serves as a basis for comparison with other similar experiments where the complete velocity gradient is determined. The standard deviation is 0.41, 0.38 and 0.33 for $x/x_*^{peak} = 0.57$, 0.94 and 2.04, respectively, in line with the results of Mullin & Dahm (2006) who reported a standard deviation of 0.35, Khashehchi *et al.* (2010) who reported 0.3 and Ganapathisubramani *et al.* (2007) who reported 0.25.

RESULTS

General Flow Structures

Figure 3 shows a sample of the iso-surfaces of enstrophy (ω^2) corresponding to 8% of the maximum found in the reconstructed volume around $x/x_*^{peak} = 0.57$. The intermittency of areas with concentrated vorticy is noticeable in this figure.

We now try to assess the broad range of excited turbulent scales in each region. To that end we use the second order structure function, i.e. $< \delta u^2(r) >$ where $\delta u(r) = u(x) - u(x+r)$ in terms of the streamwise fluctuating velocity component $u(x)$ evaluated in the reconstructed volume from Taylor's hypothesis and normalized by the Taylor microscale. Figure 4a shows the second order structure function of the entire volume at location $x/x_*^{peak} = 0.57$. There is no clear 2/3 power law range in this location.

We now follow the same approach as Mouri *et al.* (2008) and analyse sub-volumes of the entire reconstructed volume. One might expect that in highly vortical regions (such as the one in $-2550 < x/\eta < -2050$, see figure 3) there is a broader range of excited scales with a Kolmogorov-like scaling exponent closer to 2/3 than in less

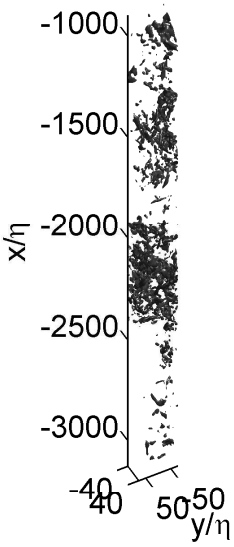

Figure 3. Iso-surfaces of enstrophy for 8% of the maximum enstrophy found at this location. Volume reconstructed from Taylor's hypothesis for $x/x_*^{peak} = 0.57$.

active regions. However, this is not the case at $x/x_*^{peak} = 0.57$ where we found that the broadest range of scales with a close to 2/3 power law is located upstream of a highly vortical region such as $-3050 < x/\eta < -2550$ in figure 3. For this particular region figure 4b shows that the second-order structure function adopts, for more than one decade, a power law with a Kolmogorov 2/3 exponent. The structure function with the same maximum size r in the region $-2550 < x/\eta < -2050$ (high enstrophy region) does not show a 2/3 power law (see figure 4c). This feature is different from what is found in Mouri *et al.* (2008) where smaller sub-regions of the flow never display a larger power law range when compared to the whole volume. As explained in Laizet *et al.* (2013) the conditions for universal equilibrium and for the Kolmogorov theory to be valid are not obviously present at the location $x/x_*^{peak} = 0.57$. In the present experiment there is significant background turbulence (see Gomes-Fernandes *et al.* (2012)) by comparison to their clean DNS which returns a very clear 2/3 power law near the grid without having to find a well tuned sub-region for this to happen.

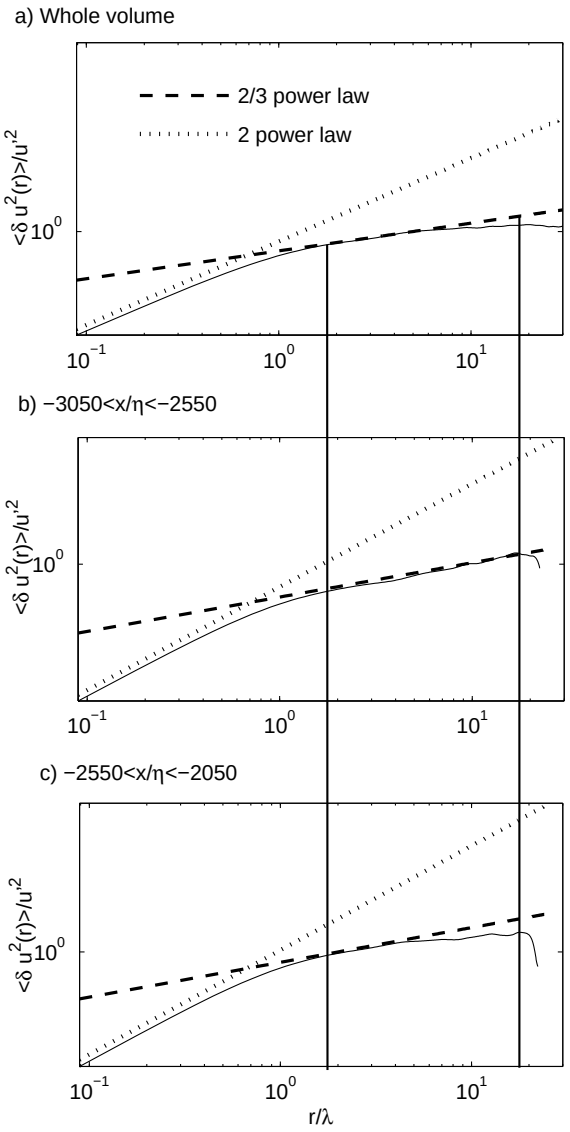

Figure 4. Second order structure function evaluated in a) entire volume, b) $-3050 < x/\eta < -2550$ and c) $-2550 < x/\eta < -2050$ (see figure 3) at $x/x_*^{peak} = 0.57$.

Invariants of the Velocity Gradient Tensor

It is useful to look at Q-R diagrams where $Q = 1/4(\omega_i\omega_i - 2s_{ij}s_{ji})$, $R = -1/3(s_{ij}s_{jk}s_{ki} + 3/4\omega_i s_{ij}\omega_j)$ and s_{ij} and ω_i are the strain rate and vorticity, respectively, of the velocity fluctuations. It has been suggested (first by Chacin & Cantwell (2000) and then by Tsinober (2009)) that this diagram has an universal tear drop shape due to the appearance of that shape in many turbulent flows such as boundary layers, mixing layers, grid turbulence and jet turbulence (see Tsinober (2009)). It is fair to question whether universal equilibrium and universal tear drop of the Q-R diagram are somehow related.

In line with what Laizet *et al.* (2013) report we present in figure 5 the spatial evolution of the Q-R diagram for the three stations studied in the present paper, $x/x_*^{peak} = 0.57$, 0.94 and 2.04. To the best of our knowledge, this is the first time a spatial development of these statistics is presented from experimental data. For the region where $x/x_*^{peak} =$ 2.04 the Q-R diagram is similar to the ones obtained in the aforementioned references with the classical tear drop shape. This information should not be taken lightly because it is in this very same region that we find the unusual scaling for the dimensionless energy dissipation constant ($C_\varepsilon = 2\nu < s_{ij}s_{ji} > L/u'^3$) with fractal grids and yet the Q-R diagram does not show any difference from the ones with classical energy dissipation scaling.

For classical tear drop shape Q-R diagrams, the areas dominated by strain (where $Q < 0$) are in general producing more gradients of the strain type than the vorticity type ($R > 0$) which gives rise to the typical tail shape of the diagram. However, the Q-R diagram at $x/x_*^{peak} = 0.57$ shows that in strain dominated regions the prevalence of strain production regions ($R > 0$) over enstrophy production ones ($R < 0$) is not as evident as at $x/x_*^{peak} = 2.04$. It is important to highlight that a region exists at $x/x_*^{peak} = 0.57$ with a 2/3

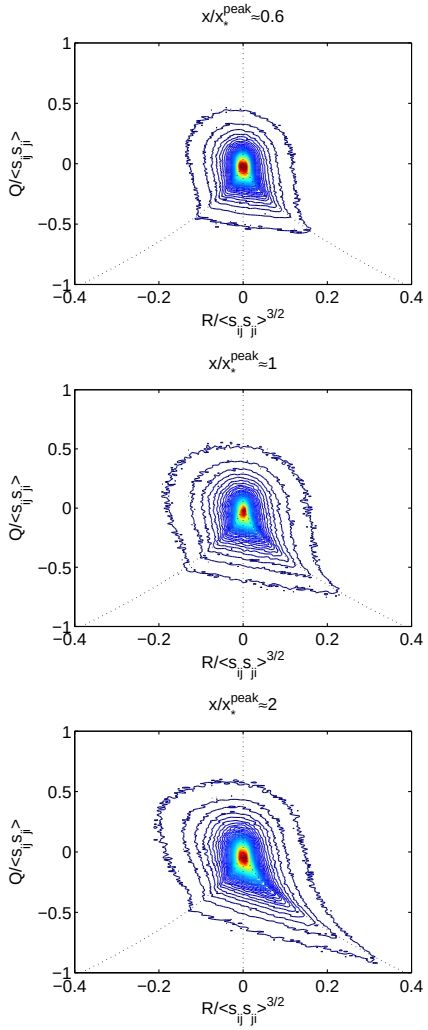

Figure 5. Spatial evolution of the Q-R diagram. The contour levels range from 10^0 to 10^{-3}.

power law in the second order structure function over more than one decade of turbulent scales (figure 4b) even though the Q-R diagram has not reached the classical shape. The measurement station located at the peak of turbulence intensity in the streamwise direction, $x/x_*^{peak} = 0.94$, shows a transiting Q-R diagram where a more pronounced tail is noticeable and larger velocity gradients appear.

We define $Q = Q_s + Q_\omega$ where $Q_s = -1/2 s_{ij}s_{ji}$ and $Q_\omega = 1/4\omega^2$ and $R = R_s + R_\omega$ where $R_s = -1/3 s_{ij}s_{jk}s_{ki}$ and $R_\omega = -1/4\omega_i\omega_j s_{ij}$. For homogeneous turbulence it can be proved that $< Q >= 0$ and $< R >= 0$. Mazellier & Vassilicos (2010) showed that at $x/x_*^{peak} \leq 1$ the flow is significantly non-homogeneous and Seoud & Vassilicos (2007), Mazellier & Vassilicos (2010) and Valente & Vassilicos (2011) showed that it is approximately homogeneous at $x/x_*^{peak} > 1$ as far as the mean flow and turbulence profiles are concerned but not as far as third order statistics such as pressure and turbulence transport terms are concerned (at least up to a distance from the grid not yet explored). Nevertheless, our statistics show that $< Q > \approx 0$ and $< R > \approx 0$ at all our three positions before, near and after x_*^{peak}. The behaviours of $< Q_s >$ and $< Q_\omega >$ and $< R_s >$ and $< R_\omega >$ which add up to zero are shown in figures 6 and 7.

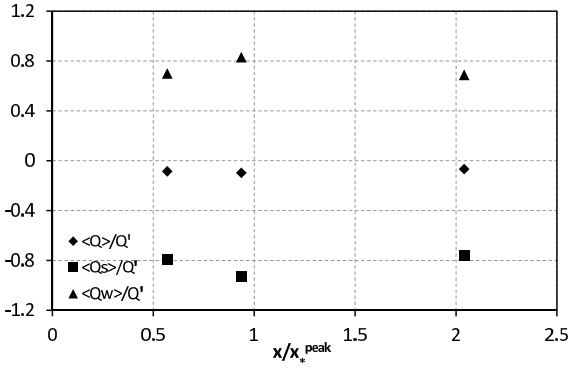

Figure 6. Spatial evolution of $< Q >$, $< Q_s >$ and $< Q_\omega >$ normalised by the root mean square of Q.

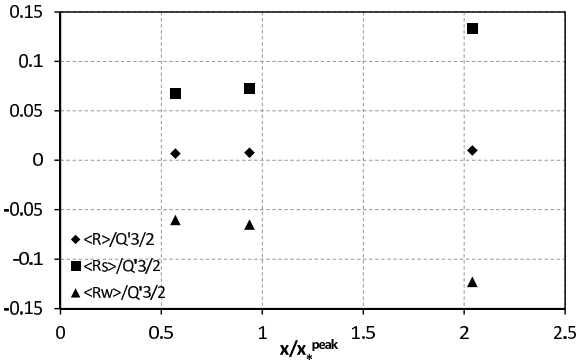

Figure 7. Spatial evolution of $< R >$, $< R_s >$ and $< R_\omega >$ normalised by the root mean square of Q to the power of 3/2.

Alignments

Another example of the universal characteristic of turbulent structures is the alignment between vorticity (ω) and the eigenvectors of the strain rate tensor (e_i for i=1 to 3). The first eigenvector (e_1) is associated with the extensive eigenvalue ($\lambda_1 > 0$), the second eigenvector (e_2) with the either extensive or compressing eigenvalue (λ_2) and the third eigenvector (e_3) with the compressive eigenvalue ($\lambda_3 < 0$). The behaviour usually reported (see, for example, Ashurst *et al.* (1987), Ruetsch & Maxey (1992) and Tsinober (2009)) is that vorticity is most likely aligned with the second eigenvector, that there is no preferential alignment with the stretching eigenvector and that it is misaligned with the compressive eigenvector.

Figure 8 shows the alignments for the three flow regions studied. Even though vorticity is most likely aligned with the second eigenvector, it starts by being slightly misaligned with the stretching and compressive eigenvector and evolves to the aforementioned usual behaviour. The behaviour seen in the production region has implications in the enstrophy production rate and, therefore, vortex stretching, as

$$\omega_i\omega_j s_{ij} = \omega_i^2 \lambda_i cos^2(\omega, e_i) \qquad (1)$$

The largest contribution to vortex stretching comes from the first (largest) eigenvalue (see table 2) even though vorticity is mainly aligned with the second one. This is due to the fact the second eigenvalue can be both posi-

Table 2. Contribution to the total mean of enstrophy production rate from the terms corresponding to the eigenvectors e_i of the strain rate tensor of the velocity fluctuations. The contribution from each eigenvector is normalized by $< \omega_i \omega_j s_{ij} >$. The values of the regular grid case were taken from Tsinober (2009) and the field experiment in atmospheric surface layer case from Kohlmyansky *et al.* (2001).

x/x_*^{peak}	0.57	0.94	2.04	Reg. Grid	Field
Re_λ	271	364	257	75	10^4
$< \omega_1^2 \lambda_1 cos^2(\omega, e_1) >$	3.2	3.65	1.58	1.17	1.44
$< \omega_2^2 \lambda_2 cos^2(\omega, e_2) >$	0.42	0.33	0.39	0.39	0.47
$< \omega_3^2 \lambda_3 cos^2(\omega, e_3) >$	-2.62	-2.98	-0.96	-0.56	-0.97

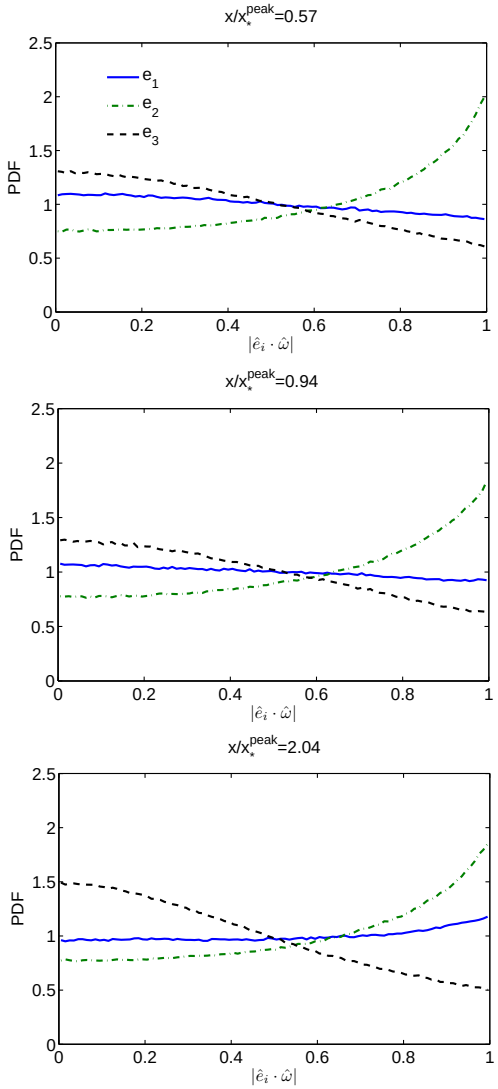

Figure 8. Spatial evolution of the alignments.

tive or negative which results in a small contribution of $< \omega_2^2 \lambda_2 cos^2(\omega, e_2) >$ to the overall enstrophy production.

Table 2 shows the contributions to the mean enstrophy production rate from the different eigenvectors of the strain rate tensor for the regions studied as well as for a reference case of a regular grid turbulence taken from Tsinober (2009) and a field experiment in atmospheric surface layer taken from Kohlmyansky *et al.* (2001). The regular grid and field experiment serve as references to conclude that the contributions of the stretching and compressive eigenvectors to the total mean of the enstrophy production rate are high at x/x_*^{peak}=0.57 and 0.94. At x/x_*^{peak}=2.04 values comparable to the reference cases are recovered.

The ratio $< \omega_1^2 \lambda_1 cos^2(\omega, e_1) > / |< \omega_3^2 \lambda_3 cos^2(\omega, e_3) >|$ (which relates the strength of vortex stretching over compression) at, for instance, $x/x_*^{peak} = 0.57$ is equal to 1.2 where for the regular grid case is 2.1. This reveals that, in station $x/x_*^{peak} = 0.57$, the vortex stretching is only slightly favoured over compression. This behaviour comes from the unusually high magnitude of the stretching and compressive eigenvalues (see table 3) given that the vorticity is initially not aligned with these eigenvectors (see figure 8). It may be particularly interesting to compare stations $x/x_*^{peak} = 0.57$ and $x/x_*^{peak} = 2.04$ as they have very similar local Re_λ values and similar PIV resolutions. Yet, in station $x/x_*^{peak} = 2.04$ the vortex stretching and compressing are comparable to the field experiment of Kohlmyansky *et al.* (2001).

Table 3 shows the ratios between $< \lambda_i^3 >$ and $- < s_{ij} s_{jk} s_{ki} >$ for the regions studied and the aforementioned atmospheric field experiment. For the production and peak regions of the fractal grid there are stronger events (relative to the mean level of strain production at each station) by comparison to the decay region and the field experiment.

Table 3. Ratios between $< \lambda_i^3 >$ and $- < s_{ij} s_{jk} s_{ki} >$. The values of the field experiment in atmospheric surface layer case were taken from Kohlmyansky *et al.* (2001).

x/x_*^{peak}	0.57	0.94	2.04	Field
$< \lambda_1^3 >$	4.54	4.54	1.57	1.62
$< \lambda_2^3 >$	0.05	0.05	0.06	0.05
$< \lambda_3^3 >$	-5.59	-5.59	-2.63	-2.67

At $x/x_*^{peak} = 0.57$, and specifically in the sub-volume $-3050 < x/\eta < -2550$, the alignments are very similar to the entire volume seen in figure 8 and the mean vortex stretching is practically the same as seen in table 2. Nevertheless, in this sub-volume we find a well defined 2/3 power law over a clear significant range (figure 4b). An attempt to differentiate this specific sub-volume from the rest of the

volume in terms of high vortex stretching and enstrophy production rate $\alpha = \omega_i \omega_j s_{ij}/\omega^2$ structures was not possible. It is therefore fair to question the importance of vortex stretching in the generation of Kolmogorov-type power law exponents.

CONCLUSIONS

An experiment regarding the spatial development of the turbulent flow generated by a fractal grid was presented and discussed. Time resolved cinematographic stereoscopic PIV allowed to measure all nine components of the velocity gradient tensor using Taylor's hypothesis. Three stations located in the production, peak and decay regions of turbulence intensity were studied. At the production region station there are specific structures where a broad range of turbulent excited scales appear. This phenomenon translates as a broad 2/3 power law range in the second order structure function conditioned on specific structures. Some acclaimed universal characteristics of turbulence structure were shown to be a gradually developing process throughout the production and peak regions. This should not be taken lightly given that these regions extend for 1.3m downstream of the grid in our experiment and can be as long as the grid design permits. The first universal aspect that was shown to be an evolution was the QR diagram. Its characteristic "tear-drop" shape becomes more pronounced downstream of the grid, at least until the location of our measurements in the decay region. In this region, the QR diagram has the usual "tear-drop" shape even though it is this region where the unusual C_ε scaling is found. The second point on universal aspects of turbulence structures is the alignment between vorticity and the eigenvectors of the strain rate tensor. The stretching eigenvector starts by being slightly misaligned with vorticity in the production region station and ends up slightly aligned with it in the decay region station. High values of the eigenvalues in the production region station has implications for vortex stretching which is stronger in this station than in the decay one.

REFERENCES

Ashurst, W. T., Kerstein, A. R., Kerr, R. M. & Gibson, C. H. 1987 Alignment of vorticity and scalar gradient with strain rate in simulated navier-stokes turbulence. *Phys. Fluids* **30**, 2343–2353.

Chacin, J. M. & Cantwell, B. J. 2000 Dynamics of a low Reynolds number turbulent boundary layer. *J. Fluid Mech.* **404**, 87–115.

Discetti, S., Ziskin, I. B., Astarita, T., Adrian, R. J. & Prestridge, K. P. 2013 PIV measurements of anisotropy and inhomogeneity in decaying fractal generated turbulence. *Fluid Dynamics Research* accepted.

Ganapathisubramani, B., Lakshminarasimhan, K. & Clemens, N. T. 2007 Determination of complete velocity gradient tensor by using cinematographic stereoscopic PIV in a turbulent jet. *Exp. Fluids* **42**, 923–939.

Gomes-Fernandes, R., Ganapathisubramani, B. & Vassilicos, J. C. 2012 Particle image velocimetry study of fractal-generated turbulence. *J. Fluid Mech.* **711**, 306–336.

Hurst, D. & Vassilicos, J. C. 2007 Scalings and decay of fractal-generated turbulence. *Phys. Fluids* **19** (035103).

Khashehchi, M., Elsinga, G. E., Ooi, A., Soria, J. & Marusic, I. 2010 Studying invariants of the velocity gradient tensor of a round turbulent jet across the turbulent/nonturbulent interface using tomo-piv. In *Proceedings of the 15th International Symposium on Applications of Laser Techniques to Fluid Mechanics 2010*. Springer Verlag.

Kohlmyansky, M., Tsinober, A. & Yorish, S. 2001 Velocity derivatives in the atmospheric surface layer at $Re_\lambda = 10^4$. *Phys. Fluids* **13**, 311–314.

Laizet, S., Vassilicos, J. C. & Cambon, C. 2013 Interscale energy transfer in decaying turbulence and vorticity-strain rate dynamics in grid-generated turbulence. *Fluid Dynamics Research* accepted.

Mazellier, N. & Vassilicos, J. C. 2010 Turbulence without Richardson-Kolmogorov cascade. *Phys. Fluids* **22** (075101).

Mouri, H., Hori, A. & Takaoka, M. 2008 Fluctuations of statistics among subregions of a turbulence velocity field. *Phys. Fluids* **20**, 035108.

Mullin, J. A. & Dahm, W. J. A. 2006 Dual-plane stereo particle image velocimetry measurements of velocity gradient tensor fields in turbulent shear flow. i. accuracy assessments. *Phys. Fluids* **18**, 035101.

Nagata, K., Sakai, Y., Suzuki, H., Suzuki, H., Terashima, O. & Inaba, T. 2013 Turbulence structure and turbulence kinetic energy transport in multiscale/fractal-generated turbulence. *Phys. Fluids* submitted.

Ruetsch, G. R. & Maxey, M. R. 1992 Small-scale features of vorticity and passive scalar fields in homogeneous isotropic turbulence. *Phys. Fluids* **3**, 1587–1597.

Seoud, R. E. & Vassilicos, J. C. 2007 Dissipation and decay of fractal-generated turbulence. *Phys. Fluids* **19** (105108).

Tsinober, A. 2009 *An informal conceptual introduction to turbulence*. New York: Springer.

Valente, P. C. & Vassilicos, J. C. 2011 The decay of turbulence generated by a class of multi-scale grids. *J. Fluid Mech.* **687**, 300–340.

Valente, P. C. & Vassilicos, J. C. 2012 Universal dissipation scaling for non-equilibrium turbulence. *Phys. Rev. Lett.* **108**, 214503.